

THE ARAKAWA JACOBIAN METHOD AND A FOURTH-ORDER ESSENTIALLY NONOSCILLATORY SCHEME FOR THE BETA-PLANE BAROTROPIC EQUATIONS

ABDERRAHIM KACIMI, TARIK ALIZIANE, AND BOUALEM KHOUIDER

Abstract. In this paper we use the Arakawa Jacobian method [1] and the fourth-order essentially non-oscillatory (ENO-4) scheme of Osher and Shu [15] to solve the equatorial beta-plane barotropic equations. The Arakawa Jacobian scheme is a second order centred finite differences scheme that conserves energy and enstrophy. The fourth-order essentially non-oscillatory scheme is designed for Hamilton-Jacobi equations and traditionally used to track sharp fronts. We are interested in the performance of these two methods on the barotropic equations and determine whether they are adequate for studying the barotropic instability. The two methods are tested and compared on two typical exact solutions, a smooth Rossby wave-packet and a discontinuous shear, on the long-climate scale of 100 days. The numerical results indicate that the Arakawa Jacobian method conserves energy and enstrophy nearly exactly, as expected, captures the phase speed the Rossby wave, and achieves an overall second order accuracy, in both cases. The same properties are preserved by the ENO-4 scheme but the fourth order accuracy is observed only for the smooth Rossby wave solution while in the case of the discontinuous shear, it yields an overall third order accuracy, even in the smooth regions, away from the discontinuity.

Key words. Arakawa Jacobian, Essentially non-oscillatory schemes, Spectral methods, Finite difference, Large scale equatorial waves, Atmospheric circulation, Barotropic flow, Vorticity, Stream function.

1. INTRODUCTION

One of the important strategies for understanding atmospheric general circulation is to study the numerical solutions of its governing equations. The equatorial beta-plane barotropic equations, a simple atmospheric model, have been studied for more than half a century and are at the heart of a hierarchy of more complex models. The first successful numerical weather prediction model, used by Charny *et al* in 1950 [3], was based on the barotropic vorticity equation (BVE). A barotropic atmosphere is a single-layered fluid; under this assumption there is no vertical component, and hence the equation to be solved is two dimensional (2D). For theoretical investigation of the evolution of vortices, atmospheric researchers are still using the barotropic assumption. For example, the BVE is useful for modelling the movement of tropical cyclones [2]. The barotropic assumption is also used to model global wave patterns in the middle troposphere [19]. To model tropical cyclones, the computational domain is a midlatitude β -plane. The β -plane approximation is a linear approximation to the Coriolis parameter found by Taylor expansion [10] for small displacement in latitude. Scale analysis show that the nonlinear term is negligible.

Most numerical models of the BVE use finite differences or spectral methods. A recent state of the art method from the applied mathematics [13] to the problem of

Received by the editors January 18, 2012 and, in revised form, June 29, 2012 .

2000 *Mathematics Subject Classification.* 35L99, 65M05, 65M06, 92.60.Bh, 92.60.Dj.

The research of A.K is supported by the Scholar Research program 2010-2012 from the Algerian Government and of T.A is supported by CNEPRU N° B00220090010, (Algeria), and B.K is partly funded by the Natural Sciences and Engineering Research Council of Canada.

tropical climate modelling [12] showed that a non-oscillatory central scheme can accurately model equatorial waves without undue dissipation of energy but seems to suffer some serious shortcoming [12, 4] (see conclusion section). However, the Arakawa Jacobian scheme [1], which is specifically designed for the incompressible BVE, is widely used in the atmosphere-ocean community. The Arakawa Jacobian has the useful feature that both domain integrated enstrophy and domain integrated kinetic energy are conserved. It also conserves mean wavenumber; this prevents nonlinear instabilities from occurring. The third method which we can adapt to solve the incompressible BVE is the high-order essentially non-oscillatory scheme (ENO) of Osher and Shu [15]. The ENO scheme is a high order accurate finite difference scheme designed for problems with piecewise smooth solutions containing discontinuities. ENO schemes are traditionally used for hyperbolic conservation laws and Hamilton-Jacobi equations [15]. The key idea lies at the approximation level, where a nonlinear adaptive procedure is used to automatically choose the locally smoothest stencil, hence avoiding crossing discontinuities in the interpolation procedure as much as possible. ENO schemes have been quite successful in applications, especially for problems containing both shocks and complicated smooth solution structures, such as compressible turbulence simulations and aeroacoustic. The paper is organized as follows. In section 2, we present the barotropic equations on the equatorial β -plane. In Sections 3 and 4, we study the numerical methods needed for solving the equatorial beta-plane barotropic equations. The Arakawa Jacobian is used together with the second-order numerical solution of the Poisson equation, used to enforce the incompressibility constraint. The fourth-order essentially non-oscillatory (ENO-4) scheme is coupled with a fourth-order Poisson solver. We validate the numerical methods in Section 5, and a summary with conclusion is presented in Section 6.

2. The Barotropic Equations on an Equatorial β -plane

In standard nondimensional units, that are defined below, the barotropic equatorial β -plane equations, for the horizontal velocity, \mathbf{v} , and pressure, p , are given by

$$(1) \quad \begin{cases} \frac{\partial \mathbf{v}}{\partial t} + \mathbf{v} \cdot \nabla \mathbf{v} + y \mathbf{v}^\perp + \nabla p = 0, \\ \operatorname{div} \mathbf{v} = 0. \end{cases}$$

In (1), $\mathbf{v} = (u, v)$ with u, v are respectively the zonal (east-west) and meridional (north-south) velocity components. The operator $\nabla = \left(\frac{\partial}{\partial x}, \frac{\partial}{\partial y} \right)$ is the horizontal gradient vector and $\operatorname{div} \mathbf{v} = \frac{\partial u}{\partial x} + \frac{\partial v}{\partial y}$ is the horizontal divergence while the term $y \mathbf{v}^\perp = y(-v, u)$ represents the horizontal components of the Coriolis force due to the vertical component of Earth's rotation (beta effect). The nonlinear equations for the barotropic mode in (1) is derived from the full 3d geophysical flow equations by assuming a rigid lid and flat bottom, constant density and hydrostatic balance. These assumptions are sufficient to neglect the vertical velocity and viscosity in the rotating Boussinesq equations [5, 14].

The equations in (1) were nondimensionalized by using the characteristic units of equatorial synoptic scale dynamics [5, 14], so that the Coriolis gradient at the equator is normalized to $\beta = 1$: the velocity scale is the gravity wave speed $c =$

$NH_T/\pi \approx 50 \text{ ms}^{-1}$ with $N = 10^{-2} \text{ s}^{-1}$ is the Brunt-Väisälä frequency, and $H_T = 16 \text{ km}$ is the tropospheric height. The length scale choice is based on the equatorial Rossby wave deformation radius $L_e = (c/\beta)^{\frac{1}{2}} \approx 1500 \text{ km}$ and the time scale is given by $T = L_e/c = (c\beta)^{-\frac{1}{2}} \approx 8.3 \text{ hours}$.

2.1. Barotropic Equations in Vorticity Stream Form. For convenience, the system in (1) is often written in vorticity-stream function form [12]:

$$(2) \quad \begin{cases} \frac{\partial \xi}{\partial t} + J(\psi, \xi) = 0, \\ \Delta \psi = \xi - y, \\ u = -\frac{\partial \psi}{\partial y}, v = \frac{\partial \psi}{\partial x}. \end{cases}$$

Here $\xi = \frac{\partial v}{\partial x} - \frac{\partial u}{\partial y} + y$ is the potential vorticity, that is the relative vorticity, $\frac{\partial v}{\partial x} - \frac{\partial u}{\partial y}$, due the flow velocity plus the vertical component of Earth's rotations, βy , and ψ is the stream function; the velocity field is given by $u = -\frac{\partial \psi}{\partial y}$, $v = \frac{\partial \psi}{\partial x}$. The term $J(\psi, \xi)$ is the Jacobian determinant with $J(\psi, \xi) = \frac{\partial \psi}{\partial x} \frac{\partial \xi}{\partial y} - \frac{\partial \psi}{\partial y} \frac{\partial \xi}{\partial x}$ represents the advective non-linearity of potential vorticity, ξ by the associated flow.

2.2. Conservation properties. For our problem, we will restrict the domain to a rectangular strip which is periodic in x . This domain is centred on the equator and represents the tropics, our principal region of interest. The north-south walls are located at a distance $Y = 5000 \text{ km}$ away from the equator and the zonal period is equal to the perimeter of the earth at the equator, i.e., $X = 40000 \text{ km}$. We assume there is no-flow through the boundaries:

$$(3) \quad v(x, \pm Y, t) = 0,$$

then from (2) the mean potential vorticity satisfies

$$(4) \quad \frac{d}{dt} \mathcal{Z} = \frac{d}{dt} \int_0^X \int_{-Y}^Y \xi dx dy = 0,$$

is conserved (independent of time t). Under the same conditions, the total enstrophy,

$$(5) \quad \zeta(t) = \frac{1}{2} \int_0^X \int_{-Y}^Y \left(\frac{\partial v(x, y, t)}{\partial x} - \frac{\partial u(x, y, t)}{\partial y} \right)^2 dx dy,$$

and kinetic energy

$$(6) \quad E(t) = \frac{1}{2} \int_0^X \int_{-Y}^Y (u^2(x, y, t) + v^2(x, y, t)) dx dy,$$

are also conserved. The conservation of ζ and E implies that the mean wavenumber of the flow is conserved [1]. In Khouider and Majda [12], the equations in (2) are solved by the non-oscillatory central scheme of Levy and Tadmor [13]. Here we propose to develop other high order and highly conservative numerical methods for the barotropic equations in (2) to compare and analyze the behavior of some simple exact and asymptotic solution to the barotropic equations. Namely we consider two

different numerical approaches: The Arakawa Jacobian method [1], which conserves both energy and enstrophy and a fourth-order ENO scheme [15].

3. The Arakawa method for barotropic waves

3.1. Free Equatorial Barotropic Vorticity Equation. The free equatorial barotropic vorticity equation can be alternatively written in an advective form

$$(7) \quad \frac{\partial \xi}{\partial t} + u \frac{\partial \xi}{\partial x} + v \frac{\partial \xi}{\partial y} = 0,$$

or in the conservative form,

$$(8) \quad \frac{\partial \xi}{\partial t} + \frac{\partial (u\xi)}{\partial x} + \frac{\partial (v\xi)}{\partial y} = 0.$$

Even though it is simple to code the advective form (7) is not typically used in practice because it does not have any obvious conservative properties and can result in instabilities which can grow with time. The numerical treatment of the conservative form, on the other hand, allows solutions that contain shocks. Khouider and Majda [12] adapted a central scheme [13] using both the advective and conservative forms (7)-(8) to avoid this problem. A piecewise approximation at each time step using staggered averaging results in smooth numerical fluxes, thereby avoiding discontinuous Riemann fans. The results of Khouider and Majda [12] are used as a benchmark to validate the two methods considered here. We consider the vorticity-stream function equation in the generic form,

$$(9) \quad \frac{\partial \xi}{\partial t} + J(\psi, \xi) = 0.$$

Under suitable boundary conditions, this equation has the useful feature of conserving both domain integrated enstrophy and domain integrated kinetic energy. It is natural to desire these same conservation properties during the discretization of the Jacobian in the (9). In addition of conserving these important physical quantities, this would guaranty the stability of the numerical scheme. The method used in [12] insures stability by relying on the machinery of high-resolution method for conservation laws. The Arakawa Jacobian method on the other hand achieves stability by conserving energy and enstrophy.

3.2. Arakawa Jacobian. A naive way to discretize the Jacobian would be to use centred differences to approximate the derivatives of

$$(10) \quad J_1(\psi, \xi) = \frac{\partial \psi}{\partial x} \frac{\partial \xi}{\partial y} - \frac{\partial \xi}{\partial x} \frac{\partial \psi}{\partial y}.$$

However, it was noted by Phillips [16] that this scheme is subject to instabilities stemming from the misrepresentation of wavelengths shorter than two grid intervals. This misrepresentation is called aliasing. It is not due to a poor choice of boundary conditions or to an inappropriately large time step but is rather an inherent feature of the scheme. The instabilities resulting from aliasing can grow without bound in a finite amount of time.

Alternatively, one would discretize either of the following equivalent formulations of the Jacobian.

$$(11) \quad \begin{aligned} J_2(\psi, \xi) &= \frac{\partial}{\partial x} \left(\psi \frac{\partial \xi}{\partial y} \right) - \frac{\partial}{\partial y} \left(\psi \frac{\partial \xi}{\partial x} \right), \\ J_3(\psi, \xi) &= \frac{\partial}{\partial y} \left(\xi \frac{\partial \psi}{\partial x} \right) - \frac{\partial}{\partial x} \left(\xi \frac{\partial \psi}{\partial y} \right). \end{aligned}$$

Using a judicious combination of J_1 , J_2 and J_3 , Arakawa was able to propose a discrete Jacobian that conserves the numerical analogues of the domain-integrated kinetic energy, domain-integrated enstrophy, and average wave number. We introduce the standard notation of centred differences:

$$\begin{aligned}\delta_i(\psi)^j &= \psi_{i+1,j} - \psi_{i-1,j}, \\ \delta_j(\xi)^i &= \xi_{i,j+1} - \xi_{i,j-1}.\end{aligned}$$

The most obvious discretization of the Jacobian is given by

$$(12) \quad J_{++}(\psi, \xi) = \frac{1}{\Delta x \Delta y} \left(\delta_i(\psi)^j \delta_j(\xi)^i - \delta_j(\psi)^i \delta_i(\xi)^j \right),$$

which corresponds to centered differences of continuum form $J_1(\psi, \xi)$. The flux form Jacobian,

$$(13) \quad J_{+\times}(\psi, \xi) = \frac{1}{\Delta x \Delta y} \left(\delta_i(\psi \delta_j(\xi)^i)^j - \delta_j(\psi \delta_i(\xi)^j)^i \right),$$

corresponds to the continuum form $J_2(\psi, \xi)$ and the flux form Jacobian,

$$(14) \quad J_{\times+}(\psi, \xi) = \frac{1}{\Delta x \Delta y} \left(\delta_j(\xi \delta_i(\psi)^j)^i - \delta_i(\xi \delta_j(\psi)^i)^j \right),$$

corresponds to the continuum form $J_3(\psi, \xi)$. Arakawa [1], showed that J_{++} preserves the symmetry, $J_{++}(\psi, \xi) = -J_{++}(\xi, \psi)$, $J_{+\times}(\psi, \xi)$ conserves the domain integrated enstrophy, $\int \xi^2 dx dy$ and $J_{\times+}(\psi, \xi)$ conserves the integral of energy, $\int \nabla \psi \cdot \nabla \psi dx dy$. As a consequence, he proved that the combination

$$(15) \quad J = \frac{1}{3} (J_{++} + J_{+\times} + J_{\times+}),$$

conserves both energy and enstrophy as well as the mean wavenumber, which as already mentioned, prevents numerical instabilities from occurring. This is what is called the Arakawa Jacobian.

3.3. Basic discretization. On a uniform grid with grid points $(x_i, y_j) = (x_0 + ih, y_0 + jh)$ $i = 0, \dots, N, j = 0, \dots, M$, we can discretize (2) in space by second-order centered finite differences combined with a second order Runge-Kutta predictor-corrector method in time:

$$(16) \quad \frac{\xi_{i,j}^{n+1} - \xi_{i,j}^n}{\Delta t} + J_{i,j}^n(\psi, \xi) = 0,$$

$$(17) \quad \Delta_{i,j}^n \psi^n = \frac{\psi_{i+1,j}^n - 2\psi_{i,j}^n + \psi_{i-1,j}^n}{\Delta x^2} + \frac{\psi_{i,j+1}^n - 2\psi_{i,j}^n + \psi_{i,j-1}^n}{\Delta y^2} = \xi_{i,j}^n - y_j.$$

Here $J_{i,j}^n$ is the Arakawa Jacobian given in (15). The use of the Arakawa Jacobian ensures conservation of discrete analogues of (4), (5) and (6), as detailed in [1]. $\Delta_{i,j}^n$ is the usual five-point approximation of the Laplacian. The Arakawa method for the barotropic system (2) is achieved by combining the discretization equation of potential vorticity in (16) with a solver for the stream-function Poisson equation in (17). We solve the difference equation in (17) by combining the FFT method for the periodic x -direction and a direct method in y [12]. The Poisson equation in (17) is closed by the periodic boundary conditions in x and the Neumann boundary condition in y ,

$$(18) \quad \frac{\partial \psi}{\partial x}(x, \pm Y) = 0,$$

dictated by the no-flow condition in (3). The Fourier method,

$$(19) \quad \psi_{i,j} = \sum_{k=1}^N \hat{\psi}_{k,j} \exp(I(i-1)(k-1)2\pi\Delta x), \quad I^2 = -1,$$

applied to the difference equation in (17), leads to a tridiagonal system for each Fourier mode with the homogeneous Dirichlet boundary conditions, $\hat{\psi}_{k,0} = \hat{\psi}_{k,M} = 0$, for all the modes, $2 \leq k \leq N$, except for the first mode, $k = 1$. We obtain a boundary condition for the first mode by relying on the conservation of the zonal mean wind at the north-south boundaries. In fact, the zonal averaging of the equation in (7) combined with the no-flow condition in (3) leads to [12]

$$(20) \quad \frac{\partial}{\partial t} \left(\frac{1}{X} \int_0^X u(x, y, t) dx \right) = 0 \text{ at } y = \pm Y.$$

This condition is used during the coding of the Poisson solver. The complete algorithm for solving the barotropic system (1) is as follows: From ξ^n , compute ψ^n by inverting $\Delta_{i,j}^n \psi^n = \xi^n - y$, compute the Jacobian $J^n(\psi^n, \xi^n)$ then compute $\xi^{n+1} = \xi^n - \Delta t J^n(\psi, \xi)$, increment n and repeat the cycle. Homogeneous Dirichlet boundary conditions are used at the walls for the potential vorticity,

$$(21) \quad \bar{\omega} = \xi - y = 0 \text{ at } y = \pm Y.,$$

combined with periodic boundary conditions in x . The validation of Arakawa's method is given in section 5.

4. Fourth-order Essentially Non-Oscillatory scheme for barotropic waves

4.1. ENO Interpolation . Essentially non-oscillatory schemes were developed by Harten *et al.* in 1987 [8, 9] when working on the numerical solution of nonlinear hyperbolic conservation laws (HCL). The solution of a system of HCL involves discontinuities. Interpolating across these discontinuities leads to Gibbs phenomenon which results in loss of accuracy and ultimately numerical instabilities. The ENO interpolation scheme is a data dependent, nonlinear reconstruction technique which can eliminate the Gibbs phenomenon. ENO schemes for Hamilton-Jacobi equations were developed in [15]. The key idea is an adaptive stencil interpolation which automatically selects the locally smoothest region, and hence yields a uniformly high-order essentially non-oscillatory approximation for piecewise smooth functions. Given point values $G(x_j)$, $j = 0, \pm 1, \pm 2, \dots$ of a (piecewise smooth) function G at discrete nodes x_j , we associate an m -th degree polynomial $P_m^{j+\frac{1}{2}}$ with each interval $[x_j, x_{j+1}]$. The ENO scheme selects the smoothest possible region of the domain by choosing the $m+1$ interpolation points, in the neighbourhood of the cell $[x_j, x_{j+1}]$ (including x_j and x_{j+1}), that achieve the smallest divided differences $G[x_1, x_2, \dots, x_k]$, of all order k , $1 \leq k \leq m+1$.

The ENO interpolation procedure starts with a base stencil containing two grid points, then adaptively adds one point to the stencil at each stage, which is either the left neighbouring point or the right neighbouring point to the current stencil depending on which would yield a smaller divided differences value. The ENO interpolation procedure results in a high order approximation that avoids spurious oscillations. More precisely, we can show that the total variation of the interpolation polynomial is at most $O(\Delta x^r)$, $r > 0$ larger than the total variation of the piecewise smooth function being interpolated. Thus the ENO procedure is especially suited

for problems with singular but piecewise smooth functions, such as solutions of nonlinear conservation laws and Hamilton-Jacobi equations. When combined with an exact or approximate Riemann solver the ENO reconstruction results in a TVB (total variation bounded) stable numerical scheme.

High-order ENO schemes for Hamilton-Jacobi equations use a monotone flux as a building block and the ENO interpolation procedure to approximate the left and right derivatives at the cell center. For the barotropic equations in (1), we propose to adapt the fourth-order ENO scheme introduced and used in [15] by Osher and Shu for Hamilton-Jacobi equations. The advective form of the potential vorticity equation (7) is thus regarded as a Hamilton-Jacobi equation:

$$(22) \quad \frac{\partial \xi}{\partial t} + H(\xi_x, \xi_y) = 0,$$

where $H(\xi_x, \xi_y)$ represents the Hamiltonian of ξ :

$$(23) \quad H(\xi_x, \xi_y) = -\frac{\partial \psi}{\partial y} \frac{\partial \xi}{\partial x} + \frac{\partial \psi}{\partial x} \frac{\partial \xi}{\partial y}.$$

Both the conservative and advective forms were exploited in [12] where the central scheme for conservation laws is used.

Remark 4.1. *In Khouider and Majda [12], the barotropic vorticity equation is solved by the central incompressible scheme of Levy and Tadmor [13], using both the advective form in (7) and the conservative form in (8). The design of this scheme is based on a predictor corrector scheme that takes advantage of the fact that the barotropic vorticity equation can be alternatively written in both forms. The conservative form justifies the use of the finite volume method during the correction step while the advective form highlights the finite-speed of propagation and is used to advance the scheme during the prediction step. The interested reader is referred to [13] for more details. While the Arakawa Jacobian insures stability by conserving energy and enstrophy, the central incompressible scheme used in [12] insures stability by relying on the machinery of high-resolution methods for conservation laws. As demonstrated in [12], the central scheme captures accurately the solution of the rotating barotropic equations on an equatorial beta-plane but it suffers from a phase lagging problem; The numerical Rossby wave solution propagates slower than its exact analog.*

4.2. Scheme construction. For mesh sizes $\Delta x, \Delta y, \Delta t$, the numerical approximation to the potential vorticity solution ξ of (22) is denoted $\xi_{i,j}^n$. We also use the standard notation

$$\xi_{x,i,j}^\pm = \pm \frac{(\xi_{i\pm 1,j} - \xi_{i,j})}{\Delta x}, \quad \xi_{y,i,j}^\pm = \pm \frac{(\xi_{i,j\pm 1} - \xi_{i,j})}{\Delta y}.$$

The numerical scheme for the equation of the potential vorticity in (22), in its Euler form, is

$$(24) \quad \frac{\xi_{i,j}^{n+1} - \xi_{i,j}^n}{\Delta t} = -H_{LLF}^n(\xi_{x,i,j}^+, \xi_{x,i,j}^-, \xi_{y,i,j}^+, \xi_{y,i,j}^-)$$

where H_{LLF}^n is the local Lax Friedrichs numerical Hamiltonian [15]:

$$H_{LLF}^n(\xi_x^+, \xi_x^-, \xi_y^+, \xi_y^-) = H\left(\frac{\xi_x^+ + \xi_x^-}{2}, \frac{\xi_y^+ + \xi_y^-}{2}\right) - \frac{1}{2}\alpha^x(\xi_x^+, \xi_x^-)(\xi_x^+ - \xi_x^-) - \frac{1}{2}\alpha^y(\xi_y^+, \xi_y^-)(\xi_y^+ - \xi_y^-)$$

Table 4.1. Coefficients of a TVD Runge-Kutta scheme for the ENO-4 scheme [15].

$\alpha_{k,l}$				$\beta_{k,l}$			
1				$\frac{1}{2}$			
$\frac{1}{2}$	$\frac{1}{2}$			$-\frac{1}{4}$	$\frac{1}{2}$		
$\frac{1}{9}$	$\frac{2}{9}$	$\frac{2}{3}$		$-\frac{1}{9}$	$-\frac{1}{3}$	1	
0	$\frac{1}{3}$	$\frac{1}{3}$	$\frac{1}{3}$	0	$\frac{1}{6}$	0	$\frac{1}{6}$

and

$$\alpha^x = \max_{\substack{r \in I(\xi_x^-, \xi_x^+) \\ C \leq q \leq D}} |H_1(r, q)|, \quad \alpha^y = \max_{\substack{q \in I(\xi_y^-, \xi_y^+) \\ A \leq r \leq B}} |H_2(r, q)|,$$

which is a Lipschitz continuous monotone flux consistent with H in PDE (22) [7]:

$$H_{LLF}^n(r, r, s, s) = H(r, s).$$

Here $H_i(r, q)$ is the partial derivative of H with respect to the i -th argument, or the Lipschitz constant of H with respect to the i -th argument. Monotonicity here means that H_{LLF}^n is nonincreasing in its first and third arguments and nondecreasing in the other two ($H_{LLF}^n(\downarrow, \uparrow, \downarrow, \uparrow)$). The scheme (24) with a monotone numerical Hamiltonian is called a monotone scheme. It is proven in [7] that monotone schemes converge to the viscosity solution of (22). We now begin the description of the fourth-order ENO scheme. The monotone flux described above play the role of building blocks. The ENO interpolation described in subsection 4.1 is used to compute fourth-order approximations to the left and right derivatives ξ_x^\pm and ξ_y^\pm . The fourth order centred differences is used to compute fourth-order approximations to the derivatives ψ_x and ψ_y . These values are then put into the monotone flux $H_{LLF}^n(\xi_x^+, \xi_x^-, \xi_y^+, \xi_y^-)$. Time accuracy is obtained by a class of TVD Runge-Kutta type time discretizations [6, 17, 18]. The algorithm can be summarized as follows: (1) At any node (x_i, y_j) , fix j to compute a derivative along the x -direction, by using the ENO interpolation procedure

$$\xi_x^\pm = \frac{d}{dx} P_4^{j \pm \frac{1}{2}}(x_i).$$

(2) Similarly, at the node (x_i, y_j) , fix i to compute along the y -direction, by using the ENO interpolation procedure

$$\xi_y^\pm = \frac{d}{dy} P_4^{i \pm \frac{1}{2}}(y_j).$$

Then let

$$L_{i,j} = -\Delta t H_{LLF}^n(\xi_x^+, \xi_x^-, \xi_y^+, \xi_y^-),$$

(3) obtain ξ^{n+1} from ξ^n by the following forth-order Runge-Kutta method:

$$(25) \quad \begin{aligned} \xi_{i,j}^{(0)} &= \xi_{i,j}^n, \\ \xi_{i,j}^{(k)} &= \sum_{l=0}^{k-1} (\alpha_{k,l} \xi_{i,j}^{(l)} + \beta_{k,l} L_{i,j}^{(l)}), \quad k = 1, 2, 3, 4, \\ \xi_{i,j}^{(n+1)} &= \xi_{i,j}^{(4)}, \end{aligned}$$

where $\alpha_{k,l}$ and $\beta_{k,l}$ are given in Table 4.1.

The method (25) can be proven total variation diminishing, under the CFL condition:

$$(26) \quad \frac{\Delta t}{\min(\Delta x, \Delta y)} \leq C_4 \lambda_0$$

where

$$\lambda_0 = \frac{1}{\max(u, v)} \text{ and } C_4 = \frac{2}{3}.$$

As remarked in [15], when implementing the ENO-4 interpolation described in subsection 4.1 we use undivided differences [15]:

$$(27) \quad \phi(i, j, 0) = \xi_{i,j},$$

for $k = 1, 5$

$$(28) \quad \phi(i, j, k) = \phi(i + 1, j, k - 1) - \phi(i, j, k - 1).$$

The computation of (28) can be easily vectorized. The ENO stencil-choosing process is as follows. For computing ξ_x^+ , starting with $k_{\min}^1 = i$

$$\text{if } |\phi(k_{\min}^1 - 1, j, k)| < |\phi(k_{\min}^1, j, k)|,$$

then

$$k_{\min}^1 = k_{\min}^1 - 1,$$

for $k = 2, 3, 4$ where k_{\min}^1 is the leftmost point in the stencil for $P_4^{j+\frac{1}{2}}(x)$. This can also be vectorized. Finally,

$$(\xi_x)_{i,j}^+ = \frac{1}{\Delta x} \sum_{k=1}^4 C(k_{\min}^1 - i, k) \cdot \phi(k_{\min}^1, j, k),$$

where

$$C(4, k) = \frac{1}{k!} \sum_{s=4}^{k+3} \prod_{l=4, l \neq s}^{k+3} (-l).$$

Note that the small matrix C , which is independent of ξ , is computed only once, and then stored. The fourth-order essentially non-oscillatory scheme (ENO-4) for the barotropic system (2) is achieved by combining the discrete equation of potential vorticity in (25) with a fourth-order Poisson solver for the stream-function. We use a nine point stencil for the Poisson equation:

$$(29) \quad \begin{aligned} \Delta_{i,j}^n \psi^n &= \frac{-\psi_{i+2,j}^n + 16\psi_{i+1,j}^n - 30\psi_{i,j}^n - 56\psi_{i-1,j}^n - \psi_{i-2,j}^n}{12\Delta x^2} \\ &+ \frac{-\psi_{i,j+2}^n + 16\psi_{i,j+1}^n - 30\psi_{i,j}^n + 16\psi_{i,j-1}^n - \psi_{i,j-2}^n}{12\Delta y^2} \\ &= \xi_{i,j}^n - y_j, \end{aligned}$$

$0 \leq i \leq N$ et $0 \leq j \leq M$. The method of resolution of the equation in (29) is similar to that used with second-order Poisson equation in (17) using the same boundary conditions for the stream-function in (18) and the same boundary conditions for the potential vorticity in (21).

5. Validation tests

Here, the numerical solutions of the equatorial barotropic vorticity equation using the Arakawa Jacobian and the fourth-order essentially non-oscillatory scheme are validated through known exact solutions.

Table 5.2. L^1 -norm relative error between the exact and the numerical potential vorticity using the Arakawa method.

Grid	5 days	10 days	15 days	20 days	50 days	100 days
128×75	$2.47E-02$	$4.89E-02$	$7.32E-02$	$9.82E-02$	$2.41E-01$	$4.61E-01$
256×150	$6.34E-03$	$1.25E-02$	$1.87E-02$	$2.51E-02$	$6.25E-02$	$1.24E-01$
Order	1.97	1.97	1.97	1.97	1.95	1.90

Table 5.3. Same as Table 5.2 but with the ENO-4 scheme.

Grid	5 days	10 days	15 days	20 days	50 days	100 days
128×75	$3.93E-07$	$6.97E-07$	$1.05E-06$	$1.42E-06$	$4.07E-06$	$1.08E-05$
256×150	$2.72E-08$	$4.67E-08$	$7.24E-08$	$9.86E-08$	$2.88E-07$	$7.76E-07$
Order	3.87	3.91	3.87	3.86	3.83	3.81

5.1. Rossby waves packets. We consider the Rossby wave packets used in [12]

$$(30) \quad \psi(x, y, t) = \cos(k_1 x - \omega t) \sin(k_2 y)$$

with k_1 is the zonal wavenumber, k_2 is the meridional wavenumber, and $\omega = \frac{-k_1}{k_1^2 + k_2^2}$ is the dispersion relation. These wave packets are defined on a periodic channel of zonal length $X = 40000 \text{ km}$ and meridional width $2Y = 10000 \text{ km}$ and they solve the nonlinear barotropic equations in (1) exactly. It can be seen that these wave packets have vanishing meridional velocity v at the channel walls ($y = \pm Y$) provided k_2 is chosen to be a multiple of $\frac{\pi}{Y}$. The solutions described by (30) represent a traveling wave packet which propagates in the zonal direction at the speed $\frac{\omega}{k_1}$. We set $k_1 = 8\pi/X$ and $k_2 = \pi/Y$, which we may abbreviate by writing $k_1 \equiv 4$ and $k_2 \equiv 1$. We fix the initial magnitude of the wind such that

$$\max_{x,y} \sqrt{(u^2(x, y, 0) + v^2(x, y, 0))} = 5 \text{ m/s.}$$

and we run the barotropic code described in section 3 and 4 forward in time. A CFL condition with Courant number 0.8 is used to calculate the time step Δt from the given grid spacing Δx and Δy , and velocities (u, v) . We choose $\Delta t = 0.8 \times (\min(\Delta x, \Delta y) / \max(u, v))$ in Arakawa method and $\Delta t = 0.8 \times C_4 \times (\min(\Delta x, \Delta y) / \max(u, v))$ in ENO-4 scheme. Notice that the Rossby wave packet in (30) satisfies the Dirichlet boundary condition in (21).

We report in table 5.2 the L^1 -norm relative error, with respect to the potential vorticity ξ , between the exact and numerical solutions for two different grids, 128×75 and 256×150 at six consecutive times, 5, 10, 15, 20, 50 and 100 days, using the Arakawa Jacobian method.

The same relative errors computed using the fourth-order essentially non-oscillatory scheme are shown in table 5.3. An examination of the rate of convergence, found by taking the ratio of errors of the two grids at a given time, suggests that both methods are able to capture the large scale dispersive wave with an overall second order and forth-order accuracy for Arakawa Jacobian method and forth-order essentially non-oscillatory scheme, respectively.

Energy-time series plots in Figure 5.1 show that energy remains relatively constant in time for the Arakawa method and the forth-order essentially non-oscillatory scheme, regardless of the number of grid points. In Figure 5.2, a zonal slice of the vorticity $\bar{\omega} = \xi - y$ at $y \approx 1600 \text{ km}$ at $t = 20$ days are shown for the grids 128×75

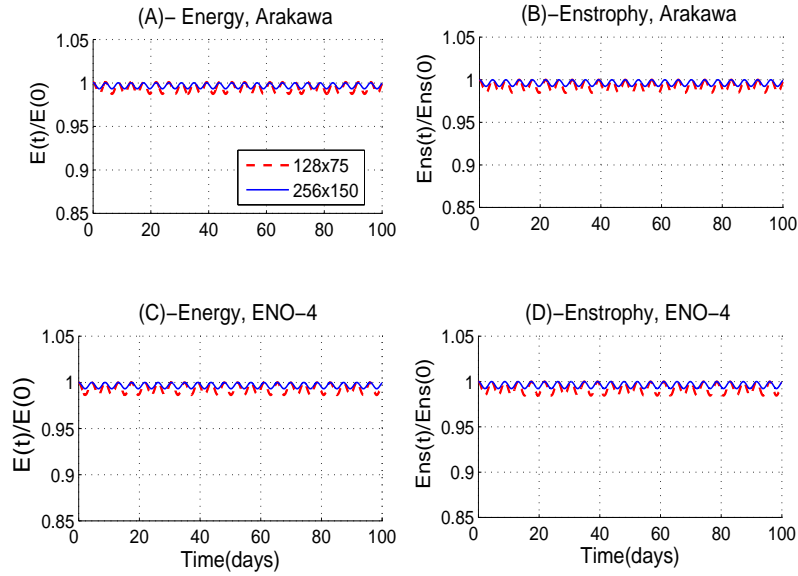


Figure 5.1. (A) and (B): Energy and Enstrophy time plots using 128x75 and 256x150 grid points using Arakawa method. (C) and (D) same as in (A) and (B) but with ENO-4 scheme.

and 256×150 using the Arakawa Jacobian method and forth-order essentially non-oscillatory scheme and is compared with the exact solution. From this plots, it is apparent that the phase speed obtained by Arakawa method and ENO-4 scheme is nearly identical of the phase speed of Rossby wave packets, unlike the central scheme that suffered from apparent phase lag [12]. Though, at coarse resolution, the Arakawa solution seems to be slightly slower that the exact wave solution while the ENO-4 method is faster. Recall that the wave is moving westward, i.e, to the left. Note that with $k_1 = 4$, there are only 32 and 64 grid points per wavelength, respectively for the two grids in figure 5.2

In figure 5.3, contour plots of the vorticity $\bar{\omega}$ are shown for the different grids and the exact solution at $t = 20$ days. Velocity profiles are also superimposed. It appears that the structure and velocity field of the wave packet is nearly identical in all three cases. The y -plots of the L^1 -norm errors in x -direction for the two grids at 5 days for both methods in figure 5.4 show that we have not an error accumulation at the walls. This is most likely due to the fact that at each time step, the Arakawa Jacobian and the Hamiltonian of $\bar{\xi}$ vanish at the boundary $y = \pm Y$.

5.2. A discontinuous shear flow. As an extreme test case, we consider a discontinuous shear flow given by

$$(31) \quad \mathbf{v} = (u(y), 0)$$

where

$$(32) \quad u(y) = \begin{cases} 1 & y > 0 \\ -1 & y < 0. \end{cases}$$

From the last equations in (2) we have:

$$u = u(y) = -\frac{\partial \psi}{\partial y} \text{ and } v = 0 = \frac{\partial \psi}{\partial x},$$

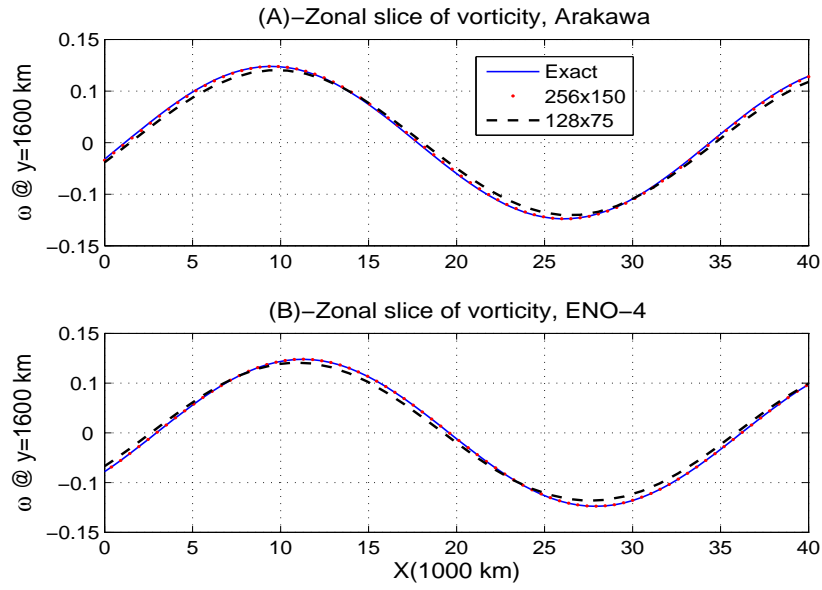


Figure 5.2. One wavelength zonal slice plot at $t=20$ days of the vorticity $\bar{\omega}$ at $y \approx 1600$ km. (A) -Arakawa method, (B)-ENO-4 scheme.

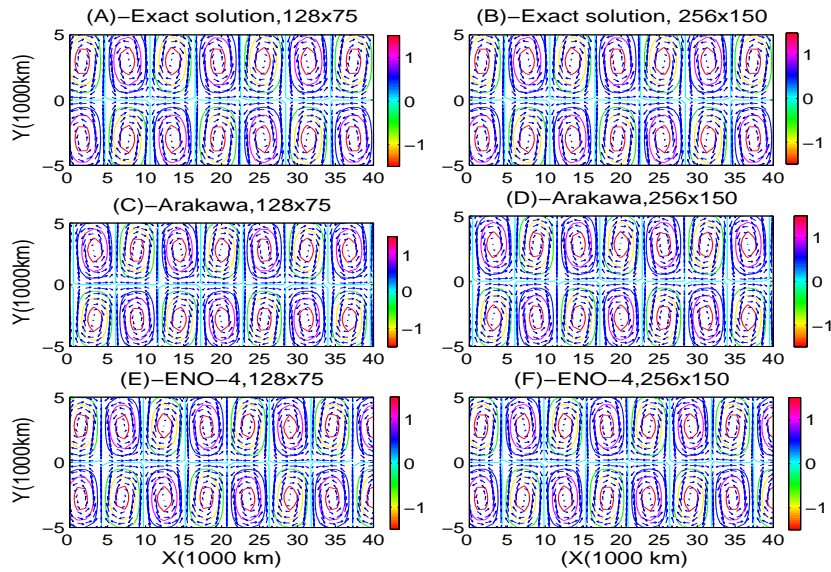


Figure 5.3. 2D structure of Rossby wave packet with $k_1 \equiv 4$ and $k_2 \equiv 1$. at time $t = 20$ days. Contours of the vorticity and velocity profile (arrows) for (C) and (D), using Arakawa method, (A) and (B) exact solution, and (E) and (F) ENO-4 scheme.

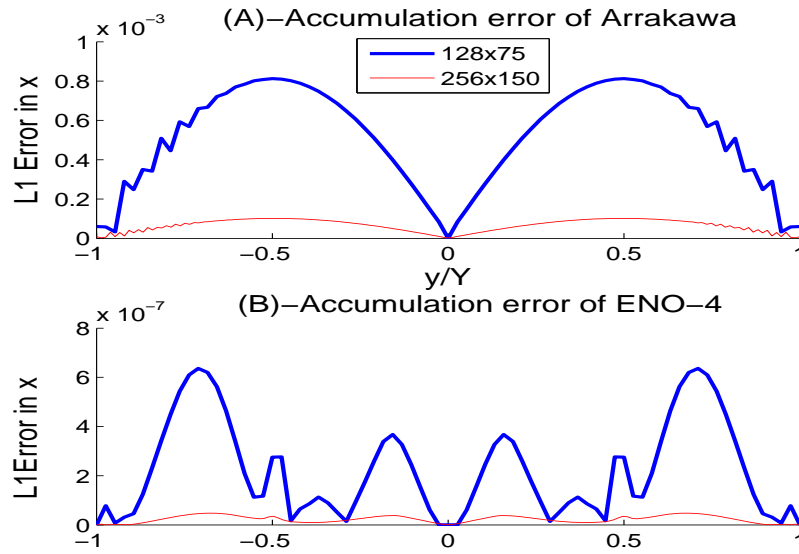


Figure 5.4. (A): L^1 -norm error in x -direction versus y at time $t = 5$ days for Arakawa method. (B): same as in (A) but with ENO-4 scheme.

which gives

$$(33) \quad \psi(y) = \begin{cases} -y & y > 0 \\ y & y < 0 \end{cases}$$

and

$$(34) \quad \xi(y) = \Delta\psi + y = -2\delta_0 + y,$$

where δ_0 is the Dirac delta function at $y = 0$. Before we proceed for validation runs, particular care needs to be taken with regards to the solutions given in (33) and (34). We note that the discontinuous shear flow is a solution to the barotropic equation in the weak sense, i.e, in the sense of distributions. Thus, the Dirac delta function is replaced by a regularization sequence (ρ_ε) , which converges towards δ_0 when $\varepsilon \rightarrow 0$. Let

$$(35) \quad \rho_\varepsilon(y) = \begin{cases} 0 & |y| > \varepsilon \\ \frac{1}{\varepsilon^2}y + \frac{1}{\varepsilon} & -\varepsilon \leq y \leq 0 \\ -\frac{1}{\varepsilon^2}y + \frac{1}{\varepsilon} & 0 \leq y \leq \varepsilon, \end{cases}$$

where ε is a small positive number. In our numerical solution, we take $\varepsilon = \Delta y$ for the second-order method that couples the Arakawa Jacobian and the second order Poisson solver, and $\varepsilon = 8\Delta y$ for the fourth-order method (ENO-4). Where Δy is the grid spacing in the North-South direction. These are the smallest ε values that work for the two methods, respectively. The ENO scheme doesn't yield the expected order of accuracy and blows up if a small perturbation is added on top of the discontinuous shear when $\varepsilon < 8\Delta y$ (results not reported here; see [11] for more details). Non-homogeneous Neumann and homogeneous Dirichlet boundary conditions are used at the wall for the stream-function and the potential vorticity, respectively:

Table 5.4. L^1 -norm relative error between the exact and the numerical streamfunction using the Arakawa method in the case of the discontinuous shear.

Grid	L_1 Error (at 20 days)	order of accuracy
64×38	$6.41E - 04$	1.88
128×75	$1.75E - 04$	2.00
256×150	$4.35E - 05$	

Table 5.5. Same as Table 5.4 but with the ENO-4 scheme. L_1 error on the whole domain and its restriction to the smooth regions $|y| > 8\Delta y$.

Grid	Whole domain		Smooth regions	
	L_1 Error	order of accuracy	L_1 Error	order of accuracy
64×38	$1.31E - 03$	2.62	$8.11E - 04$	3.22
128×75	$2.15E - 04$	2.93	$8.77E - 05$	3.26
256×150	$2.83E - 05$		$9.23E - 06$	

$$(36) \quad \frac{\partial \psi}{\partial y}(Y) = -1, \quad \frac{\partial \psi}{\partial y}(-Y) = 1$$

$$(37) \quad \bar{\omega} = \xi - y = 0 \quad \text{at } y = \pm Y.$$

We report in table 5.4 the L^1 -norm relative error, with respect to the streamfunction ψ , between the exact and numerical solutions for three different grids, 64×38 , 128×75 and 256×150 at time 20 days, using the Arakawa Jacobian method for the discontinuous shear flow. The same relative errors computed using the fourth-order essentially non-oscillatory scheme are shown in table 5.5. Note that in Table 5.5, both the L_1 error on the whole domain and its restriction to the smooth region away from $y = 0$, and the associated order of accuracy, are reported. In Figure 5.5, the smoothed vorticity and streamfunction of the "exact" and numerical solutions are shown for the grid 128×75 using the Arakawa Jacobian method. Figure 5.6 is the same as Figure 5.5 but for the ENO-4 scheme.

We note that in this case of the discontinuous shear (exact) solution, none of the schemes is expected to return its theoretical order of accuracy. However, as we can see from Tables 5.4 and 5.5 and Figures 5.5 and 5.6, both the Arakawa Jacobian and the ENO-4 methods reproduce the discontinuous shear solution with great accuracy. However, it is interesting to note here that while Arakawa's method recovers the formal second order convergence (as shown on the last column of Table 5.4), the actual order of accuracy is less than 3 i.e way below the theoretical fourth order convergence rate, unlike the smooth case in Table 5.3. This can be explained in part by the fact that the Arakawa method uses a smoother $\varepsilon = \Delta y$ while ENO-4 necessitates $\varepsilon = 8\Delta y$. But for all practical purposes, both methods seem to yield adequate results. When the error calculation for the ENO scheme is restricted to the region of the domain where the solution is smooth, we recover an order of accuracy larger than 3 but still smaller than 4. Due to the ellipticity of the Poisson equation, the numerical "inaccuracy" which is otherwise concentrated near the singularity propagates (with an infinite speed) to the rest of the domain. This explains in part why even within the smooth regions of the domain fourth order accuracy is not achieved as shown in Table 5.5.

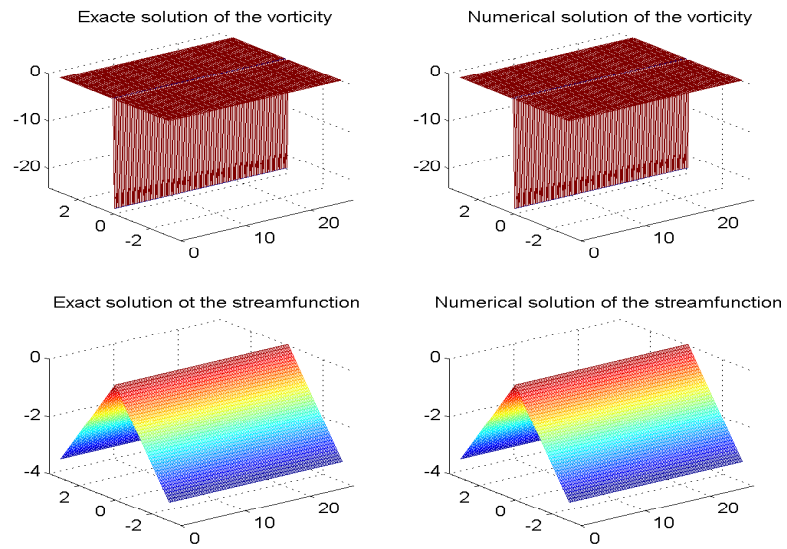


Figure 5.5. Three dimensional plots of the exact and numerical solutions, 128×75 grid points using Arakawa method in the case of the discontinuous Shear.

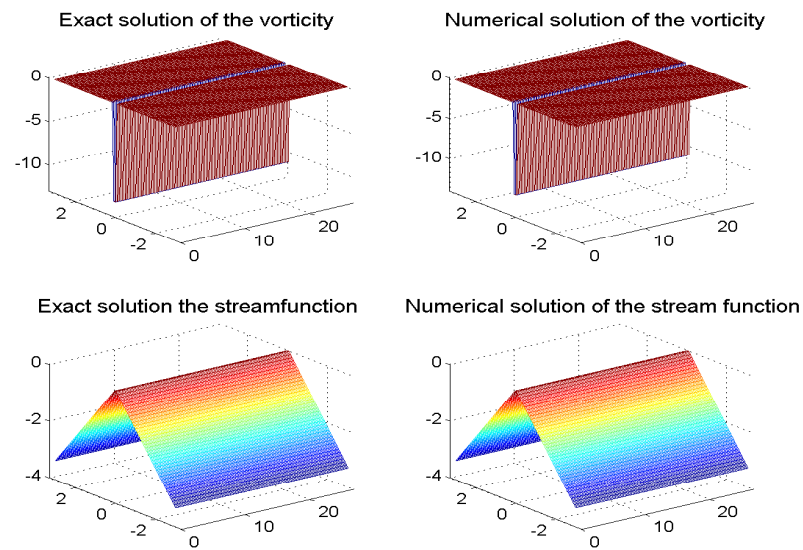


Figure 5.6. Same as in figure 5.5 but with ENO-4 scheme.

6. Summary and conclusion

This paper discusses the implementation of the Arakawa Jacobian method and the fourth-order essentially non-oscillatory scheme (ENO-4) of Osher and Shu [15] for solving the equatorial barotropic equations. The Arakawa Jacobian scheme [1]

is a second order centered finite differences scheme that conserves energy and enstrophy and it is specifically designed for the barotropic vorticity equation in (2). As such, it is widely used in the atmosphere-ocean community. The fourth-order essentially non-oscillatory scheme of Osher and Shu [15] however, is originally designed for hyperbolic conservation laws and Hamilton-Jacobi equations, and is used to track sharp fronts. Nonetheless, it can be implemented for any first order non-linear evolution PDE, and in particular for the barotropic vorticity equation in (2). The incompressible barotropic vorticity equation is considered in the advective form and solved using the Arakawa Jacobian method and the ENO-4 scheme with an explicit Runge-Kutta time integration. At each stage of the Runge-Kutta integration, the wind field was updated by solving a Poisson problem for the stream function.

In a first test, the numerical schemes for the equatorial barotropic vorticity equations using the Arakawa Jacobian and ENO-4 scheme are validated using a known Rossby wave packet solution. It is shown that as expected the Arakawa Jacobian method conserves energy and enstrophy nearly exactly and captures the dispersive wave structure of the test solution with an overall second order accuracy. The same properties are preserved by the ENO scheme and the large scale dispersive wave is captured with an overall fourth-order accuracy. In a second validation test, we considered a discontinuous shear flow with a jump discontinuity at the equator, which in theory, is an exact solution for the system (1), in the weak sense, despite the jump discontinuity. Because the vorticity of the prescribed discontinuous shear flow is a Dirac delta function, a smoothing procedure consisting of approximating the delta function with the regularizing sequence (ρ_ε) , where ε , the width of the smoothing region around the discontinuity, is set to $\varepsilon = \Delta y$ for Arakawa's method and $\varepsilon = 8\Delta y$ for the ENO-4 scheme; Δy is the grid spacing in North-South direction. An examination of the rate of convergence, found by taking the ratio of error of two grids at a given time, show that Arakawa's method reproduces the discontinuous shear solution with second order accuracy but the ENO-4 scheme is only third order accurate, for the grids used here.

Comparing the two methods, Arakawa's method is simpler to code and faster at run-time. Moreover in the case of the discontinuous shear flow, the ENO-4 scheme's order of accuracy is reduced due to the regularizing sequence (ρ_ε) , which uses a much larger ε value. A recent state of the art method for solving the barotropic vorticity equation is a non-oscillatory central scheme by Khouider and Majda [12]. They showed that the non-oscillatory central scheme can accurately model equatorial waves. However, as demonstrated in [12], the central scheme suffers from a serious problem of phase lagging. The numerical wave solution propagates slower than its exact analog. As it can be surmised from Figure 5.2, the same issue seems to occur here for Arakawa method but it is less severe than what was seen in [12]. The ENO scheme on the other hand, seems to produce a wave packet that moves slightly faster. Moreover, the central scheme has a more serious problem of distorting the shape of the wave because various parts of the wave may be lagged differently, as shown in [4] for the case of equatorially trapped waves. This is due to the systematic averaging along grid cells that characterizes the central scheme [4]. The objective of this numerical solution of the barotropic system by the two methods described in this paper is a search for an adequate numerical method to study the barotropic instability on the equatorial beta-plane. This is pursued in [11].

Acknowledgments

The research of B.K. is supported in part by the Natural Sciences and Engineering Research Council of Canada and A. K. is supported by a Government of Algeria Scholarship.

References

- [1] A. Arakawa, Computational design for long-term numerical integration of the equations of fluid motion, two-dimensional incompressible flow. *Journal of computational physics*, pp 119-143, 1966.
- [2] J. C. L. Chan, R. T. Williams, Analytical and numerical studies of the beta-effect in tropical cyclone motion. Part I, zero mean flow. *Journal of atmospheric sciences* 44(9): pp1257-1265, 1987.
- [3] J. G. Charney, R. Fjortoft, Von Neumann, Numerical integration of the barotropic vorticity equation. *Tellus* 2(4): pp 237-254, 1950.
- [4] J. Ferguson, B. Khouider, M. Namazi, Two-way interaction between equatorially-trapped waves and the barotropic flow. *Chinese Annals of Mathematics, Series B* 30: pp 2943-2975, 2009.
- [5] A. Gill, *Atmosphere-ocean dynamics*, Academic Press, New York, 1982.
- [6] S. Gottlieb, C. W. Shu, Total Variation Diminishing Runge-Kutta schemes, *Math. Comput.*, 67: pp 73-85, 1998.
- [7] M. Grandall and P. Lions, Two approximations of solutions of Hamilton-Jacobi equations, *Math. Comput.*, 43: pp 1-19, 1984.
- [8] A. Harten and S. Osher, Uniformly high order accurate non-oscillatory schemes, I. *SIAM J. numer. anal.* ,24: pp 279-309, 1987.
- [9] A. Harten, B. Engquist, S. Osher, and S. Chakravarty, Uniformly high order accurate non-oscillatory schemes, III. *J. comput. Phys.*, 71: pp 231-303, 1987.
- [10] J. R. Holton, *An introduction to dynamic meteorology* (4th edn). Elsevier Academic Press : Burlington, MA, 2004.
- [11] A. Kacimi, B. Khouider, A numerical investigation of the barotropic instability on the equatorial beta-plane. *Theoretical and Computational Fluid Dynamic*, 2011 (In press, DOI: DOI: 10.1007/s00162-012-0260-3).
- [12] B. Khouider, A. J. Majda, A non-oscillatory balanced scheme for an idealized tropical climate model. Part I: Algorithm and validation, *Theor. Comput. Fluid Dyna.* 19: pp 331-354, 2005.
- [13] D. Levy, E. Tadmor, Non-oscillatory central schemes for the incompressible 2d Euler equations. *Mathematical Research Letters* 4, pp 1-20 1997.
- [14] A. J. Majda, *Introduction to PDE and waves for atmosphere and ocean*. Courant Lecture Notes in Mathematic, vol.9. American Mathematical Society, providence 2003.
- [15] S. Osher and C. W. Shu, High-order essentially nonoscillatory schemes for Hamilton-Jacobi equations. *Siam J. Numer. Anal.*, vol. 28, No4: pp 907-922, 1991.
- [16] N.A. Phillips, An example of non-linear computational instability, the atmosphere and the sea in motion, Rossby memorial volume: pp 501-504. Rockefeller Institute Press, New York, 1959.
- [17] C. W. Shu, and S. Osher, Efficient implementation of essentially non-oscillatory shock-capturing schemes I, *Journal of Comput physic*, 77: pp 439-471 1988.
- [18] C. W. Shu, and S. Osher, Efficient implementation of essentially non-oscillatory shock-capturing schemes II, *Journal of Comput physic*, 83: pp 32-78 1989.
- [19] D. L. Williamson, Integration of the barotropic vorticity equation on a spherical geodesic grid. *Tellus*, 20(4): pp 642-653, 1968.

A. Kacimi and T. Aliziane, Department of Mathematics, Laboratory AMNEDP, University of Sciences and Technology Houari Boumedienne, Po Box 32 El-Alia, Bab Ezzouar 16079 Algiers, Algeria.

E-mail: kacimi@uvic.ca or akacimi@usthb.dz and taliziane@usthb.dz

B. Khouider, Department of Mathematics and Statistics University of Victoria, PO BOX 3045 STN CSC, Victoria, B.C., V8W 3P4, Canada.

E-mail: khouider@math.uvic.ca

URL: <http://www.uvic.ca/~khouider/>